DOI: 10.13009/EUCASS2019-512

8TH EUROPEAN CONFERENCE FOR AERONAUTICS AND AEROSPACE SCIENCES (EUCASS)

DOI: ADD DOINUMBER HERE

A Timescale-Augmented Spalart-Allmaras Turbulence Model for Flamelet Combustion Applications

Tim Horchler†, Stefan Fechter, Sebastian Karl and Klaus Hannemann
German Aerospace Center (DLR)
Institute of Aerodynamics and Flow Technology
Spacecraft Department
Bunsenstrasse 10, 37073 Göttingen, Germany
†tim.horchler@dlr.de

Abstract

Flamelet combustion models cannot be used in combination with one-equation turbulence models, e.g. the classical Spalart-Allmaras model, because they require an explicit value for the turbulent time scale. As this can be avoided for Large-Eddy simulations, Reynolds-averaged Navier-Stokes simulations and Detached-Eddy simulations rely on an explicit transport equation for the turbulent time scale.

This work extends the Spalart-Allmaras turbulence model by a transport equation for the specific dissipation rate ω borrowed from an earlier version of the Wilcox $k-\omega$ model. The new model is tested in simulations of a generic 2D test case and two model combustion chamber.

1. Introduction

The development of future space launch vehicles relies on the accurate simulation of combustion processes in rocket thrust chambers. One major engineering concern is the development of strong combustion instabilities, a phenomenon that has been investigated since the Apollo age in the 1960's but is still poorly understood today. In order to better understand the physical mechanisms triggering and sustaining such instabilities, scale-resolving simulation (e.g. Large-Eddy simulations) techniques have emerged as a promising tool to understand the processes in harsh flow environments that are difficult to investigate experimentally. The simulation of flow fields in rocket combustors requires accurate modeling of the real-gas thermodynamic states, the chemical reactions and the turbulent flow physics. In order to reduce the computational cost, we use a Detached-Eddy model in combination with a real-gas flamelet combustion model for simulating these types of flows.

While enjoying great popularity due to its simplicity and success in predicting attached boundary layer flows with good accuracy, the Spalart-Allmaras (SA) turbulence does not provide a turbulent time scale which is needed as input for flamelet combustion models. Even though there have been extensions to the original detached-eddy model formulation employing two-equation models, the Spalart-Allmaras model remains a popular choice as the background model.

During simulations of supercritical flows with high density variations, we encountered severe stability problems when using two-equation turbulence models. For detailed chemistry simulations without turbulence-chemistry interaction, these problems can be avoided by using a one-equation model, however, using a flamelet model is currently impossible due to the missing turbulent time scale in one-equation models.

This work therefore provides an extension to the Spalart-Allmaras model by using a modified ω equation from the Wilcox $k-\omega$ model thus enabling SA-based RANS and DES with flamelet combustion models.

We discuss different terms and necessary simplifications in the original ω equation for coupling it to the transport equation of the SA viscosity. A limiting approach and the formulation of boundary conditions is also discussed. The modeling approach is validated against a two-dimensional numerical test case. In a second test case, the new model is used to simulate a seven-injector gaseous CH_4/O_2 experimental combustion chamber. In a third test case, the simulation results for a model combustion chamber including real-gas effects will be shown.

DOI: 10.13009/EUCASS2019-512

2. DLR TAU Code

The DLR TAU code[9,28] is a second-order compressible finite-volume solver for flow simulations on hybrid, fully unstructured and structured meshes. TAU has been applied to a large variety of applications ranging from the low subsonic regime up to hypersonic flows.[20] The standard solver uses an edge-based dual-cell approach based on a vertex-centered scheme. Time integration is conducted using an explicit Runge-Kutta scheme and an implicit approximate factorization scheme (LUSGS).

A large variety of upwind solvers are implemented in TAU. Besides the standard TAU upwind solvers AUSMDV,[7] AUSM+UP[16] and MAPS+,[25] two recently proposed low-dissipation versions of the Roe solver named L2Roe and LMRoe[22] are implemented. An additional low Mach number correction[33] allows to greatly improve the dissipation properties of the numerical scheme at high wave numbers and assures the correct scaling of density and pressure fluctuations in the limit of Ma$\rightarrow$ 0.

TAU has also been extended allowing for scale resolving simulations by using various Large- and Detached-Eddy models.[17,18] These models have also been successfully applied to fundamental investigations of launch vehicle aerodynamics.[12]

Real-gas thermodynamic properties of gas mixtures are modeled using the multi-fluid mixing approach[4] and a high-fidelity equation-of-state description.[8] Thermodynamic properties of the species are stored in an efficient quad tree-based lookup table. In addition to the tabulation approach, TAU can also use a cubic equation of state[14] (i.e. Soave-Redlich-Kwong and Peng-Robinson) for modeling real-gas properties.

Chemical reactions can be modelled by either solving partial density transport equations for all participating species and closing the production term with a modified Arrhenius approach. Turbulence-chemistry interaction is considered by using a transport-PDF method. Alternatively, a flamelet combustion model can be employed using additional transport equations for the mixture fraction and its variance only. The flame shapes are precomputed using a separate (real-gas) flamelet equation solver (see Sec. 2.1) and stored in lookup tables. In order to further increase the speed of the simulation, transport coefficients and cubic-mixture parameters can also be included in the flamelet table.

Different one-equation, two-equation and RSM turbulence models are implemented in TAU. A detailed description of the models will be given in Sec. 4.

2.1 Flamelet Solver RGFlamelet

In order to decrease the computational time necessary for complex chemistry schemes, we use a flamelet combustion model in this work. Under the assumption of fast chemistry compared to turbulent time scales (large turbulent Damköhler numbers, the laminar flamelet equations

$$-\rho\frac{\chi}{2}\frac{\partial^2 Y_s}{\partial Z^2} = \dot{m}_s \tag{1}$$

$$-\rho\frac{\chi}{2c_p}\left(\frac{\partial^2 h}{\partial Z^2} - \sum_{s=1}^{N_s} h_s\frac{\partial^2 Y_s}{\partial Z^2}\right) = -\frac{1}{c_p}\sum_s h_s\dot{m}_s \tag{2}$$

can be derived. Their solution represents one-dimensional counter flow diffusion flames in mixture fraction Z space. The flame shape is determined by the profile of scalar dissipation rate

$$\chi(Z) = \chi_{st}\exp\left[2\left([\mathrm{erfc}^{-1}(2Z_{st})]^2 - [\mathrm{erfc}^{-1}(2Z)]^2\right)\right] \tag{3}$$

where the stoichiometric scalar dissipation rate $\chi_{st.}$ is a measure of the strain rate in the flame. Large values of χ lead to extinction while for small values we obtain chemical equilibrium flamelets.

The thermodynamic treatment of the species uses the exact same models as the DLR TAU code, i.e. cubic equations of state[14] (Soave-Redlich Kwong and Peng-Robinson), as well as a high-accuracy description using Helmholtz-energy based formulations.[8]

The chemical source term is closed by the law of mass actions

$$\dot{m}_s = M_s\sum_r(\beta_r^s - \alpha_r^s)\left[k_r^f\prod_s[X^s]^{\alpha_r^s} - k_r^b\prod_s[X^s]^{\beta_r^s}\right] \tag{4}$$

with an modified Arrhenius approach

$$k_r^f = A_r T^{n_r}\exp\left(-\frac{E_r}{RT}\right) \tag{5}$$

DOI: 10.13009/EUCASS2019-512

in case of pressure-independent reactions.

For pressure-dependant reactions, the model of Lindemann[34]

$$k_r^f = k_r^\infty \left(\frac{P_{\text{red.}}}{1 + P_{\text{red.}}} \right) F(T, P_{\text{red.}}) \tag{6}$$

is used. The reduced pressure is given by

$$P_{\text{red.}} = \frac{k_r^0 [M]}{k_r^\infty} \tag{7}$$

and requires two sets of forward-reaction coefficients k_r^∞ and k_r^0 for the modified Arrhenius equation in the high- and low-pressure limit. The Lindemann approach contains fall-off functions according to Gilbert[10] with Troe coefficients A, T_1, T_2 and T_3

$$\log_{10} F(T, P_{\text{red.}}) = \frac{\log_{10} F_{\text{cent}}(T)}{1 + f_1^2} \tag{8}$$

$$F_{\text{cent}}(T) = (1 - A) \exp\left(-\frac{T}{T_3}\right) + A \exp\left(-\frac{T}{T_1}\right) + \exp\left(-\frac{T_2}{T}\right) \tag{9}$$

$$f1 = \frac{\log_{10} P_{\text{red.}} + C}{N - 0.14(\log_{10} P_{\text{red.}} + C)} \tag{10}$$

$$C = -0.4 - 0.67 \log_{10} F_{\text{cent}} \tag{11}$$

$$N = 0.75 - 1.27 \log_{10} F_{\text{cent}} \tag{12}$$

In order to obtain a consistent second-order formulations of the discretized gradient terms, RGFlamelet uses analytically derived grid refinement functions modifying the flamelet equations by adding metric terms. The resulting nonlinear boundary value problem is then solved by an iterative Newton solver invoked from the Portable, Extensible Toolkit for Scientific Computation (PETSc).[2,3] For the inner linear problem, a Generalized Minimum Residual Method (GMRES) is used. Because of the very stiff chemistry terms, using proper preconditioning is indispensable. In this case, the incomplete lower-upper decomposition (ILU) allowed for proper convergence.

Counter flow diffusion flame results from this solver have been verified using literature results[15,19] and flamelet solutions from other software packages.[24]

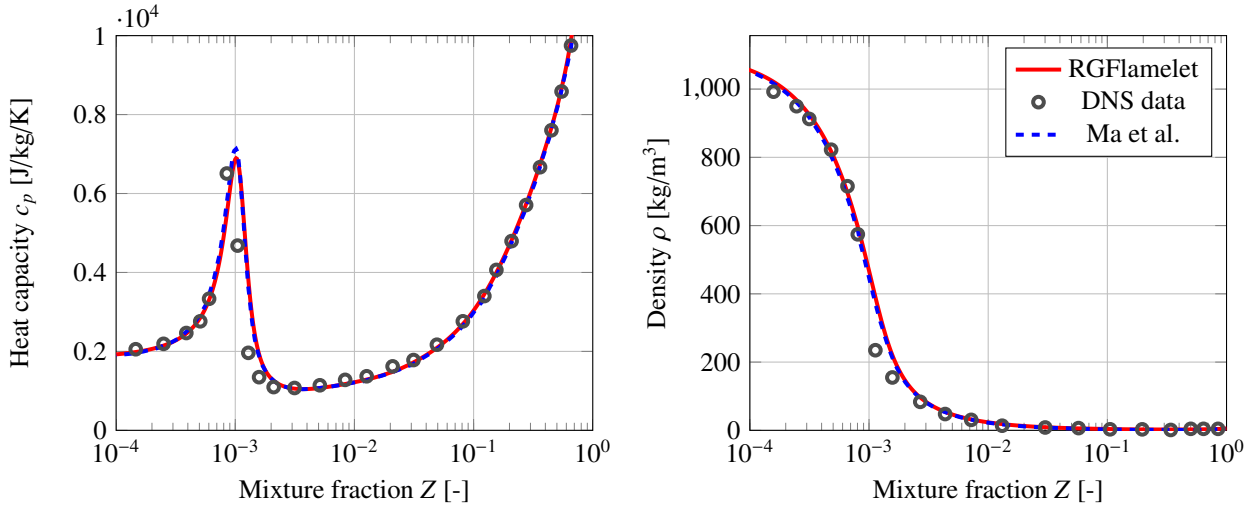

Figure 1: Validation of the real gas flamelet solver RGFlamelet using results from Ma et al.[19] and DNS data from Lacaze et al.[15] The plot shows the flame structure for a H_2/O_2 counter flow diffusion flame with transcritical oxygen injection at 70 bar.

Fig. 1 shows a comparison between results from this solver, literature results[19] for a counter flow diffusion flame and DNS data[15] for the same transcritical injection condition. The correct density profile, as well as the correct position and strength of the c_p-peak at the oxidizer side is recovered. Other variables, e.g. the temperature and the species mass fraction profiles agree also very well with the results from the literature.

DOI: 10.13009/EUCASS2019-512

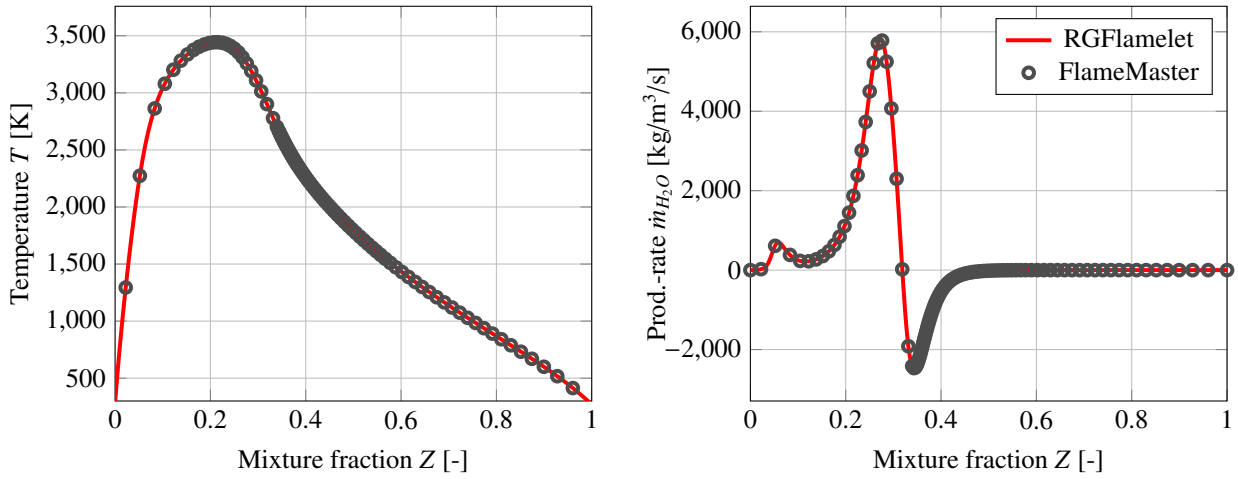

Figure 2: Validation of the ideal gas CH_4/O_2 flamelet results from RGFlamelet to the reference software FlameMaster.[24] The plot shows the flame structure for a counter flow diffusion flame at 19 bar and $\chi = 200\,\mathrm{s}^{-1}$.

In order to verify the pressure-dependant reaction approach, flamelet solutions from RGFlamelet are compared against results from FlameMaster.[24] Because there are currently no real-gas CH_4/O_2 flamelet solutions available, results are compared for ideal gas flamelets (see Fig. (2)).

Comparing both results shows an almost perfect match between the two solvers. Any species production rate is a very useful variable when it comes to comparing flamelet solutions, as it reacts highly sensitive to differences in the model implementation.

The flamelet solver is used to calculate a set of counter flow diffusion flames for stoichiometric scalar dissipation rates $\chi_{st.}$ ranging from quasi-equilibrium reactions $\chi \Rightarrow 0\,\mathrm{s}^{-1}$ to highly stretched flames for $\chi \approx 1 \times 10^5\,\mathrm{s}^{-1}$.

The results from the flamelet solver represent flame shapes for laminar counter flow diffusion flames. In order to take the effect of turbulence into account, an assumed-β-PDF approach in mixture fraction space is used to calculated the averaged species mass fractions.

The averaged species mass fraction in calculated by weighting the laminar species composition with the probability density function

$$\overline{Y}_i(\widetilde{Z}, \widetilde{Z}''^2, \chi_{st.}) = \int_0^1 Y_i(\chi_{st.}, Z) P(Z, \widetilde{Z}, \widetilde{Z}''^2)\,\mathrm{d}Z \tag{13}$$

The probability density function is assumed to be a β-PDF with mixture fraction $\widetilde{Z}$ and variance of mixture fraction $\widetilde{Z}''^2$ as its parameters:

$$P(Z, \widetilde{Z}, \widetilde{Z}''^2) = \frac{\Gamma(\gamma)}{\Gamma(\alpha)\Gamma(\beta)} Z^{\alpha-1}(1-Z)^{\beta-1}, \quad \gamma = \frac{\widetilde{Z}(1-\widetilde{Z})}{\widetilde{Z}''^2} - 1, \quad \alpha = \gamma\widetilde{Z}, \quad \beta = \gamma(1-\widetilde{Z}) \tag{14}$$

3. Flamelet Combustion Modeling

Instead of solving species transport equations for all participating species, the flamelet model only requires two additional equations irrespective of the underlying chemistry scheme.

$$\frac{\partial(\overline{\rho}\widetilde{Z})}{\partial t} + \frac{\partial(\overline{\rho}\widetilde{Z}\widetilde{u}_j)}{\partial x_j} = \frac{\partial}{\partial x_j}\left[\left(\frac{\mu}{\mathrm{Sc}} + \frac{\mu_T}{\mathrm{Sc}_T}\right)\frac{\partial\widetilde{Z}}{\partial x_j}\right] \tag{15}$$

$$\frac{\partial(\overline{\rho}\widetilde{Z}''^2)}{\partial t} + \frac{\partial(\overline{\rho}\widetilde{Z}''^2\widetilde{u}_j)}{\partial x_j} = 2\frac{\mu_T}{\mathrm{Sc}_T}\frac{\partial\widetilde{Z}}{\partial x_j}\frac{\partial\widetilde{Z}}{\partial x_j} - \overline{\rho}\chi + \frac{\partial}{\partial x_j}\left[\left(\frac{\mu}{\mathrm{Sc}} + \frac{\mu_T}{\mathrm{Sc}_T}\right)\frac{\partial\widetilde{Z}''^2}{\partial x_j}\right] \tag{16}$$

The transport equation for the mixture fraction $\widetilde{Z}$ represents the passive transport of scalar because there are no source terms involved. The mixture fraction therefore determines the mixture state of the flow. At the fuel inflow boundary, the boundary condition for the mixture fraction $\widetilde{Z} = 1$ while it is $\widetilde{Z} = 0$ on the oxidizer side.

DOI: 10.13009/EUCASS2019-512

The second additional transport equation for the variance of the mixture fraction represents fluctuations in the mixture state due to the motion of the fluid. Its destruction term contains scalar dissipation rate χ given by

$$\chi = C_\chi C_\mu \omega \widetilde{Z''^2} \tag{17}$$

with model the coefficients $C_\chi = 2$ and $C_\mu = 0.09$. It involves a turbulent time scale, in this case given by the turbulent ω from a two-equation turbulence model.

Because the turbulent time scale is unavailable from one-equation models for turbulence, we propose a simple method to augment the Spalart-Allmaras model by a passive turbulent time-scale equation.

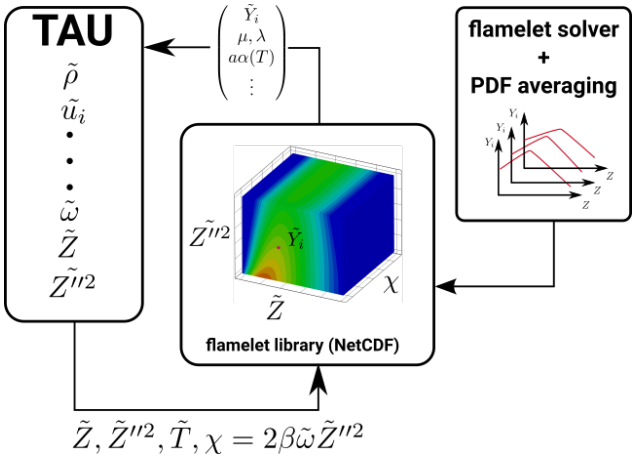

Figure 3: Flow diagram of the interaction between the TAU code, the flamelet solver and flamelet library.

The coupling between the TAU code and the flamelet library is depicted in Fig. (3). In a preprocessing step, multiple flamelet solutions for different scalar dissipation rates are PDF weighted and stored in a three-dimensional lookup table. After each solver iteration step, the primitive variables are calculated from the conservative variables. Then, $\widetilde{Z}$, $\widetilde{Z''^2}$ and χ are used to lookup the corresponding fluid composition $\overline{Y}_i$ which TAU uses in combination with the energy to iterate the fluid temperature.

In an additional step, the temperature of the fluid can be used to lookup other variables from the flamelet table to further increase the speed of the simulation. One example is the computationally expensive calculation of the laminar transport coefficients for gas mixtures because it involves n_s^2 operations[37,38] with n_s being the number of species. The same applies to the cubic mixture coefficients in case of real-gas simulations. It is sufficient to store only the linearized additional variables because there is a small difference between the correct temperature from the compressible solver and the essentially incompressible flamelet temperature.

DOI: 10.13009/EUCASS2019-512

4. Turbulence Modeling

4.1 A Turbulent Timescale Equation

The starting point for deriving a separate timescale equation for the Spalart-Allmaras model is the compressible 2006 Wilcox $k-\omega$ model.[36] The transport equation for the specific dissipation rate ω is given by

$$\frac{\partial(\overline{\rho}\omega)}{\partial t}+\frac{\partial(\overline{\rho}\omega\widetilde{u_j})}{\partial x_j}=\alpha\frac{\omega}{k}\overline{\rho}\tau_{ij}\frac{\partial\widetilde{u_i}}{\partial x_j}-\beta\overline{\rho}\omega^2+\sigma_d\frac{\overline{\rho}}{\omega}\frac{\partial k}{\partial x_j}\frac{\partial\omega}{\partial x_j}+\frac{\partial}{\partial x_j}\left[(\mu+\sigma\mu_T)\frac{\partial\omega}{\partial x_j}\right] \tag{18}$$

The transport equation is accompanied by the auxiliary relations

$$\overline{\rho}\tau_{ij}=2\mu_T\overline{S}_{ij}-\frac{2}{3}\overline{\rho}k\delta_{ij},\quad \overline{S}_{ij}=S_{ij}-\frac{1}{3}\frac{\partial\widetilde{u_k}}{\partial x_k}\delta_{ij},\quad S_{ij}=\frac{1}{2}\left(\frac{\partial\widetilde{u_i}}{\partial x_j}+\frac{\partial\widetilde{u_j}}{\partial x_i}\right),\quad \Omega_{ij}=\frac{1}{2}\left(\frac{\partial\widetilde{u_i}}{\partial x_j}-\frac{\partial\widetilde{u_j}}{\partial x_i}\right) \tag{19}$$

In this model, the turbulent eddy viscosity μ_T is calculated from the limited specific dissipation rate $\widetilde{\omega}$

$$\mu_T=\frac{\overline{\rho}k}{\widetilde{\omega}},\quad \widetilde{\omega}=\max\left(\omega,C_{\text{lim.}}\sqrt{\frac{2\overline{S}_{ij}\overline{S}_{ij}}{\beta^*}}\right),\quad C_{\text{lim.}}=\frac{7}{8}. \tag{20}$$

The transport equation (18) is closed by the following closure coefficients:

$$\alpha=\frac{13}{25},\quad \beta=\beta_0 f_\beta,\quad \beta_0=0.0708,\quad \sigma=\frac{1}{2},\quad \sigma_{do}=\frac{1}{8} \tag{21}$$

$$\sigma_d=\begin{cases}0, & \frac{\partial k}{\partial x_j}\frac{\partial\omega}{\partial x_j}\le 0\\ \sigma_{do}, & \frac{\partial k}{\partial x_j}\frac{\partial\omega}{\partial x_j}>0\end{cases},\quad f_\beta=\frac{1+85\chi_\omega}{1+100\chi_\omega},\quad \chi_\omega=\left|\frac{\Omega_{ij}\Omega_{jk}\hat{S}_{ki}}{(\beta^*\omega)^3}\right|,\quad \hat{S}_{ki}=S_{ki}-\frac{1}{2}\frac{\partial\widetilde{u_m}}{\partial x_m}\delta_{ki} \tag{22}$$

This model has evolved over time from the Wilcox 1988 model.[35] The main differences between the original version and the one presented above is the addition of the cross-diffusion term and the stress limiter Eq. 20. Regarding these modifications, Wilcox[36] states that the addition of the cross-diffusion term, suggested by Speziale,[31] reduces the model sensitivity to the free stream value of ω. Free stream sensitivity is a feature of two equation models resulting in different solutions when the first (k) and second turbulence quantity (ω, ϵ, etc.) are chosen in a way that μ_T and k are negligible. Then the solution shows sensitivity to the free stream value of the second turbulent property, in this case ω. The introduction of the stress limiter modification reduces the magnitude of the eddy viscosity in regions where the production of turbulent kinetic energy exceeds its dissipation. Basing the eddy viscosity upon $\widetilde{\omega}$ instead directly using ω improves simulation results for transonic flows.

Comparing the performance of the improved 2006 $k-\omega$ model version with the original 1988 model, Wilcox[36] notes that the original model already performs very well for attached boundary layers, mildly separated and backward-facing step flows. The main improvement over the old model is found for free shear flows and shock-separated flows.

The previous discussion now suggests a reasonable way to combine the ω-equation with the Spalart-Allmaras model by using the Wilcox 1988 model. We note that the the turbulent kinetic energy k only appears explicitly in the cross-diffusion and production term where it is found twice.

As the sole purpose of the cross-diffusion term is to reduce the free stream sensitivity of the solution to boundary values of ω, we are not expecting a large effect when neglecting this term in the ω equation. The effect of free stream sensitivity arises from the interplay between k- and the ω equation, as well as the eddy viscosity formed by the turbulent properties resulting from the transport equations. In addition to that, the original Wilcox 1988 model already showed good results for many types of flows even without the cross-diffusion term present. It appears therefore reasonable to neglect the cross-diffusion term for this type of application.

The turbulent kinetic energy appears twice in the production term. The first occurrence as a prefactor $\alpha\omega/k$ in front of the Reynolds stress tensor can be replaced by the definition of the eddy viscosity resulting in

$$\alpha\frac{\omega}{k}=\alpha\frac{\overline{\rho}}{\mu_T}. \tag{23}$$

The second occurrence of the kinetic energy k is in the isotropic part of the Reynolds stress tensor

$$p=\frac{2}{3}\overline{\rho}k. \tag{24}$$

DOI: 10.13009/EUCASS2019-512

This term acts as an additional static pressure and is also found in the Favre-averaged Navier-Stokes momentum equations. It is neglected in one-equation turbulence models because no equation for the turbulent kinetic energy is solved. Additionally, there is evidence[32] that neglecting the $2/3\overline{\rho}k$ even when using two-equation models helps in overcoming stability issues.

Solving the specific dissipation rate equation in this way reduces it to a passive additional equation. As the eddy viscosity is solely calculated from the Spalart-Allmaras equation, the ω equation can only influence the solution indirectly via the flamelet model.

In order to be consistent with the turbulence modeling setup in the DLR TAU code, we use the following parameters for the ω equation

$$\alpha = 5/9, \quad \beta = 0.075, \quad \sigma_{do} = 0 \tag{25}$$

therefore neglecting the cross diffusion term and the scaling in the production term.

In contrast to the ω limiting approach from Wilcox,[35] we follow Rudnik[26] who relates the minimum admissible ω to the free stream reference value ω_∞ by

$$\widetilde{\omega} = \max\left(\omega, \Phi^{\omega}\omega_\infty\right) \tag{26}$$

Here, the user-provided fraction Φ^{ω} is set to 10^{-5} by default. The free stream reference ω_∞ is calculated from the reference velocity u_∞, the turbulence intensity TI and the desired ratio of turbulent-to-laminar viscosity (μ_T/μ) by

$$\omega_\infty = \rho\frac{k_\infty}{\mu_{T,\infty}} = \rho\frac{1.5\left(u_\infty \cdot TI\right)^2}{\mu_\infty \cdot (\mu_T/\mu)} \tag{27}$$

4.2 Extension to a DES Flamelet Model

The transport equation for the variance of mixture fraction Eq. (16) allows for a reformulation of the destruction term in the same way as the Menter-SST $k-\omega$ is reformulated as a Detached-Eddy simulation model. Noting that the eddy viscosity in a two-equation $k-\omega$ model can be written using the turbulence length scale l

$$\mu_T = \rho C_\mu^2 \omega l^2, \tag{28}$$

we can rewrite the scalar dissipation rate as

$$\rho\chi = \rho C_\chi C_\mu \omega \widetilde{Z''^2} = \frac{C_\chi}{C_\mu}\frac{\mu_T}{l^2}\widetilde{Z''^2}. \tag{29}$$

Now, the definition of the turbulent length scale is modified such that it is taken to be the RANS length scale l_{RANS} or the LES length scale $C_{Z''^2}\Delta$:

$$l = \min(l_{\mathrm{RANS}}, C_{Z''^2}\Delta) \tag{30}$$

where Δ is the grid spacing. The DES modification of the scalar dissipation agrees, up to a factor, with the model derivation from Ihme.[13]

DOI: 10.13009/EUCASS2019-512

5. Results

In the following sections, the newly developed timescale-augmented Spalart-Allmaras model will be applied to two test cases and its performance will be assessed. All simulation results presented here use a modification of the original Spalart-Allmaras model[1] allowing for negative SA viscosities.

5.1 Simulation Results for a Generic 2D Test Case

The first test case is an ideal gas version of the purely numerical test case from Ruiz[27] which was originally used for the validation of supercritical mixing. It has been subsequently used by Ma[19] for simulating a reacting shear layer with supercritical O_2 injection. Due to its simplicity, this test case is very well suited for fundamental tests of new techniques. In order to assess the performance of the new SA-based flamelet model, the test case is reduced to an ideal gas setup with simplified chemistry.

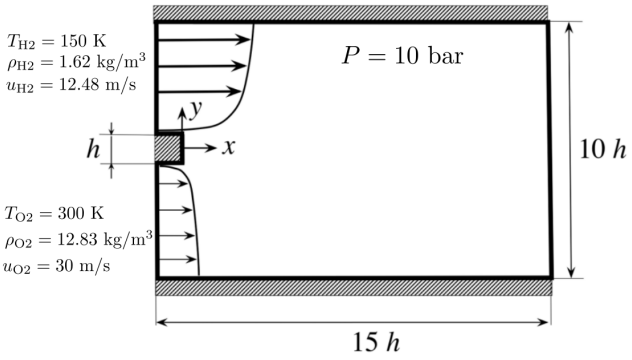

Reaction	$A\left[\frac{\text{cm}^{3(p-1)}}{\text{mol}^{p-1}K^n s}\right]$	n [-]	$E\left[\frac{J}{\text{mol}K}\right]$
Forw. k_F	2.2500×10^{18}	0.0	71128
Backw. k_B	7.6271×10^{16}	0.542299	553399

Figure 4: Numerical setup of the 2D generic test case. The table on the right shows the forward and backward rates for the one-step chemistry scheme.

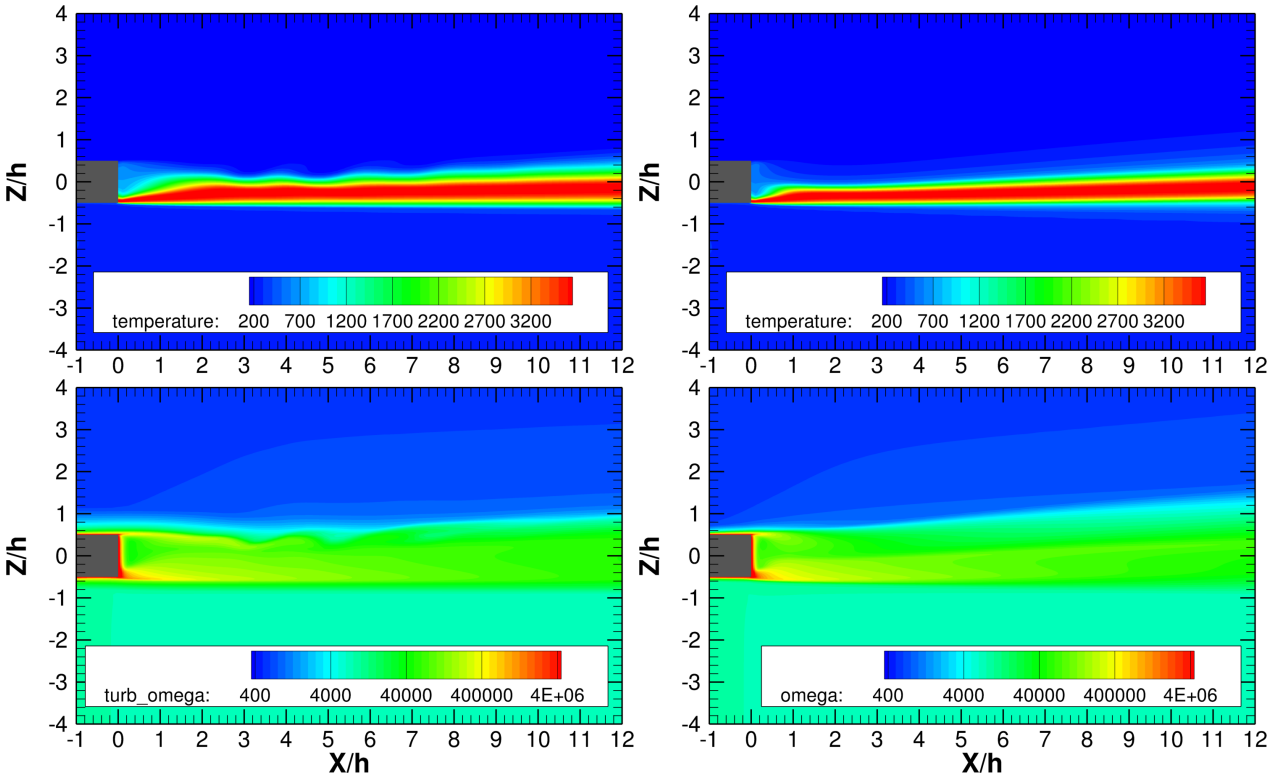

Figure 5: **Left column**: Simulation results for the two equation Wilcox 1988[35] model. **Right column**: Simulation results for the timescale-augmented Spalart-Allmaras model.

DOI: 10.13009/EUCASS2019-512

Fig. (4) shows the numerical setup. The fuel (H_2) and oxidizer (O_2) are injected with a constant mass flow rate ($\rho \cdot u_0$) at constant static temperature T over a small step of $h = 0.5$ mm which initially separates the two streams. The inflow turbulent intensity is fixed at TI = 0.1% and the boundary value ratio of laminar-to-turbulent viscosity is set to 0.1 at all inlets. Behind the splitter block, a diffusion flame forms which exits the domain downstream at an exit-pressure outflow boundary condition. The ambient pressure is set to 10 bar and a three-step reaction scheme is used.

The simulation results for the 2D generic test case are given in Fig. (5) and (6). The left column shows the two-equation $k-\omega$ simulation results, the right column the timescale-augmented Spalart-Allmaras model.

The first row of Fig. (5) shows a comparison between the flame temperature for both turbulence models. One notices that the overall flame sheet and the maximum temperature agree very well for both simulation. For the two-equation model solution (left column) one finds the onset of vortical structures indicated by the wobbly outer flame layer. As it will become apparent when comparing the ratio of turbulent-to-laminar viscosity later, the one-equation model predicts a significantly higher turbulent viscosity for this type of shear flow resulting in larger damping of unsteady features.

Row two compares the predicted turbulent ω from both models. We find a very good agreement between the two-equation $k-\omega$ model and the augmented SA-model. The result shows that the passive ω equation from the Wilcox 1998 model behaves in the same way regardless of the second turbulence equation it is coupled to.

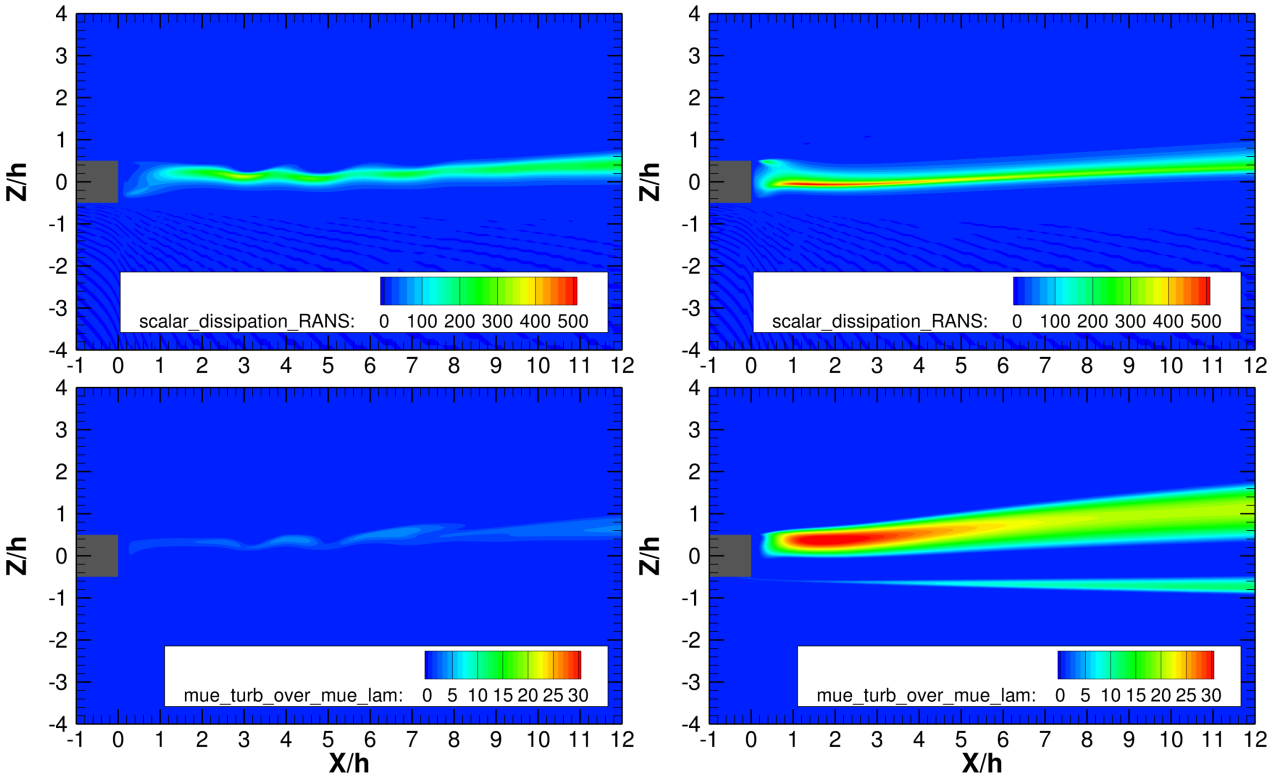

Figure 6: **Left column**: Simulation results for the two equation Wilcox 1988[35] model. **Right column**: Simulation results for the timescale-augmented Spalart-Allmaras model.

The first row of Fig. (5) compares the scalar dissipation rate Eq. (17) for both turbulence models. One notices a higher level of scalar dissipation rate for the timescale-augmented SA model compared to the Wilcox $k-\omega$ model. This can be attributed to higher variance of mixture fraction $\widetilde{Z}''^2$ (not shown) directly affecting the scalar dissipation rate.

The second row of Fig. (6) shows the ratio of turbulent-laminar-viscosity μ_T/μ indicating a quasi-laminar flow with the Wilcox $k-\omega$ model. The maximum ratio μ_T/μ does not exceed ≈ 7 in contrast to the Spalart-Allmaras model predicting a maximum ratio of ≈ 30. It must be noted, however, that the different turbulent states predicted for this type of flow are features of the underlying turbulence model and are not associated with the additional ω-equation for the Spalart-Allmaras model.

DOI: 10.13009/EUCASS2019-512

5.2 Simulation Results for the 7-Injector Test Case from TU Munich

The timescale-augmented SA model is applied to a more challenging test case from the German research program Transregio SFB-TRR 40 "Technological Foundation for the Design of Thermally and Mechanically High Loaded Components of Future Space Transportation Systems". Test case LFA-7[29] is a seven injector experimental combustion chamber using gaseous CH_4/O_2. The test case was provided by the Technical University of Munich and is specifically designed to allow for high chamber pressures up to 100 bar. The chamber walls consist of four water cooled cylindrical segments and a nozzle element for which wall temperatures and integral heat fluxes are measured. In addition to that, the pressure profiles can be measured along the combustion chamber wall. Test case LFA-7 has been simulated by five different groups during a workshop. The results are compiled by Perakis[23] and show a good agreement of the DLR-TAU results with the experimental data and results from other test case participants.

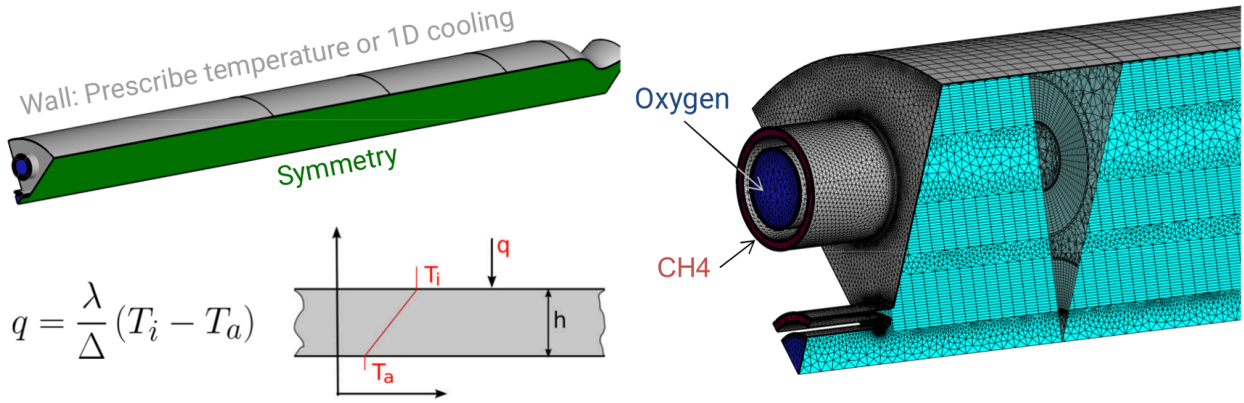

Figure 7: Numerical setup of the LFA 7 test case.

The numerical setup Fig. (7) in this work is identical to the one presented in the workshop results.[23] Simulations are run on a 60° segment of the full domain and use a hybrid mesh with a refined boundary layer grid to resolve temperature gradients properly. Constant static temperature and mass fluxes are applied at all inlet boundary conditions. The inflow boundary conditions are summarized in Tbl. (8a). The combustion chamber walls are modelled using a thermal reservoir boundary condition that links the wall heat flux to a temperature jump over a finite-thickness wall. The segment thicknesses, reservoir temperatures and heat conduction coefficients are given in Tbl. (8b).

Species	**Massflux $\dot{q}$ [kg/s]**	**Temperature T [K]**
O_2	0.211	260
CH_4	0.08	238

(a) Inflow boundary conditions.

Seg.	**Δ [mm]**	**λ [W/m/K]**	**T_a [K]**
A	2.8	100	300
B	1.3	100	300
C	1.4	100	300
D	1.3	100	300

(b) Thermal reservoir wall boundary conditions.

All simulations use a standard Flamelet model Sec. (3) with constant Schmidt and Prandtl numbers set to Sc = Pr = 0.5 (Lewis number Le =1 assumption). The flamelet tables are created using the full GRI 3.0 mechanism[30] including pressure-dependant reactions. In the following plots, simulation results using the Menter-SST model[21] are compared against the ω-augmented SA-negative model.[1]

Fig. (9) shows the pressure profiles along the combustion chamber wall for the Menter-SST and the SA-neg-ω model and compares them to the experimental results (black symbols). Both simulation results underpredict the combustion chamber pressure but follow the trend very well. The combustion chamber pressure predicted by the SA-neg-ω model agrees better with the experimental results but shows a steeper pressure drop in the first half of the chamber.

Fig. (10) shows the heat flux profiles along the combustion chamber wall. In addition to that, the segment-integrated experimental wall heat flux is shown as solid black lines. The simulation results agree very well with the experimental heat flux. In the first wall segment, the SA-neg-ω shows better results than the Menter-SST model and gives the correct integral heat flux. Further downstream, all models underestimate the heat flux except for the nozzle segment. This underestimation in the nozzle segment is attributed to large axial thermal gradients[23] caused by a high cooling water mass flow rate in this segment.

DOI: 10.13009/EUCASS2019-512

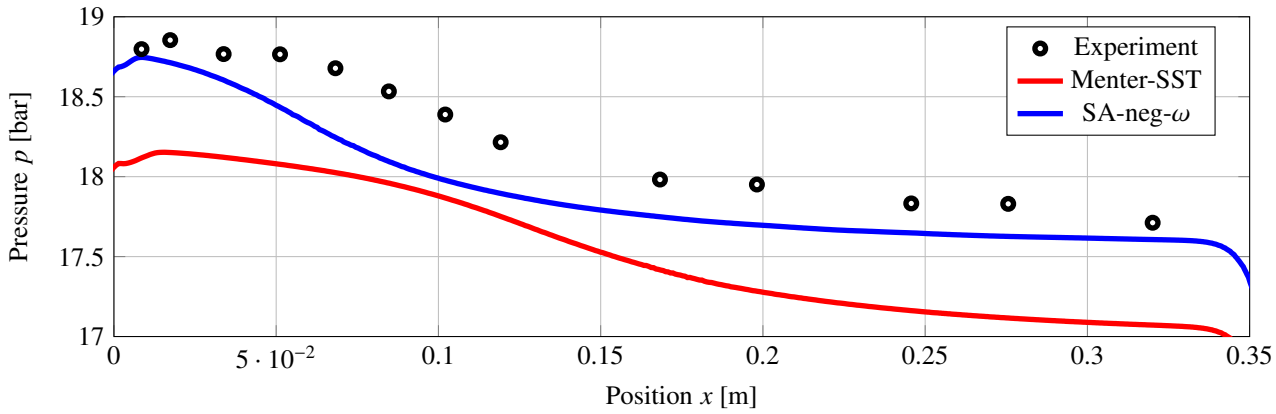

Figure 9: Comparison of the wall pressure profiles with the experimental values.

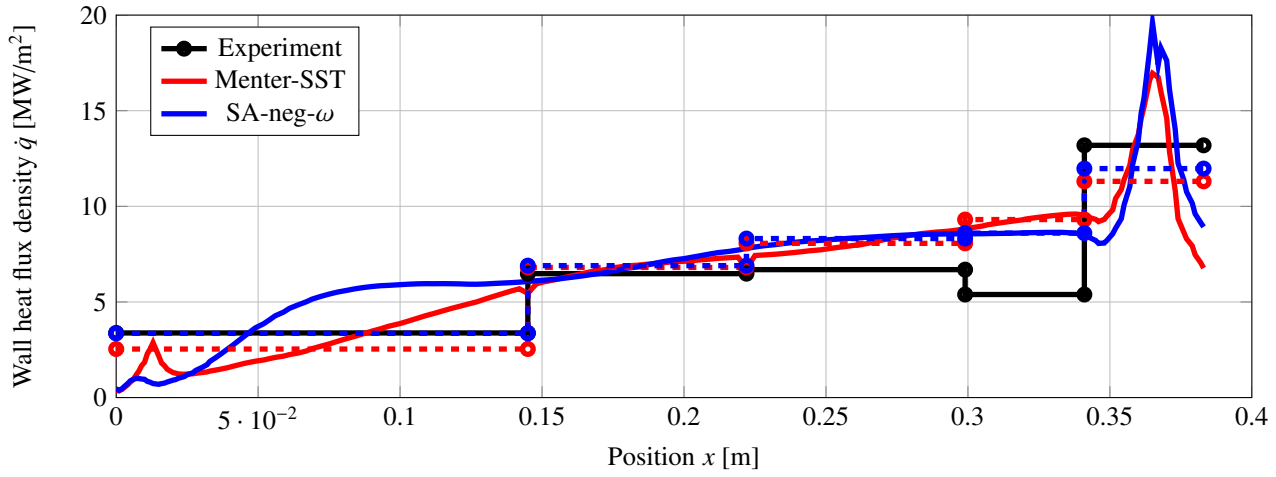

Figure 10: Comparison of the wall heat flux profiles with the experimental values. Dashed lines indicate the segment-averaged heat fluxes from the numerical simulations.

It can be stated, however, that both models predict the wall pressure and heat flux well and that the SA-neg-ω gives even slightly better results than the Menter-SST model for this test case.

5.3 Simulation Results for Combustion Chamber H

The original motivation for developing a timescale-augmented version of the Spalart-Allmaras turbulence model came from numerical stability problems with two-equation models. These instabilities were found in simulations of supercritical fluids when there were large density gradients are present in the flow.

In this section, results are presented for the application of the new model to a model combustion chamber simulation. Combustion chamber H (BKH)[5,11] from DLR Lampoldshausen is a sub scale research chamber consisting of five coaxial injectors surrounded by 50 secondary hydrogen injection elements. The combustion chamber is equipped with dynamic pressure sensors and a secondary nozzle which can be opened and closed periodically by a siren excitation wheel. The siren wheel can be used to excite combustion chamber eigenmodes. Optical access through windows on both sides of the chamber allow for recording OH^* emission and shadowgraphy images which help to better understand the flame dynamics.

The steady RANS simulation is run with the timescale-augmented SA flamelet model using the 6 species 7 reaction Burke[6] mechanism. Supercritical O_2 and H_2 injection is modeled using the Soave-Redlich-Kwong equation of state[14] with the single-fluid mixing model. Oxygen is injected at 125.5 K while the hydrogen injection temperature is 61.9 K. The simulation is run using a 3D half model grid consisting of 7.6 million grid points. We used an low-Mach-number improved[33] MAPS+ upwind scheme[25] for calculating the numerical fluxes.

The qualitative comparison between the experimental and the numerical results shows a good agreement for the

DOI: 10.13009/EUCASS2019-512

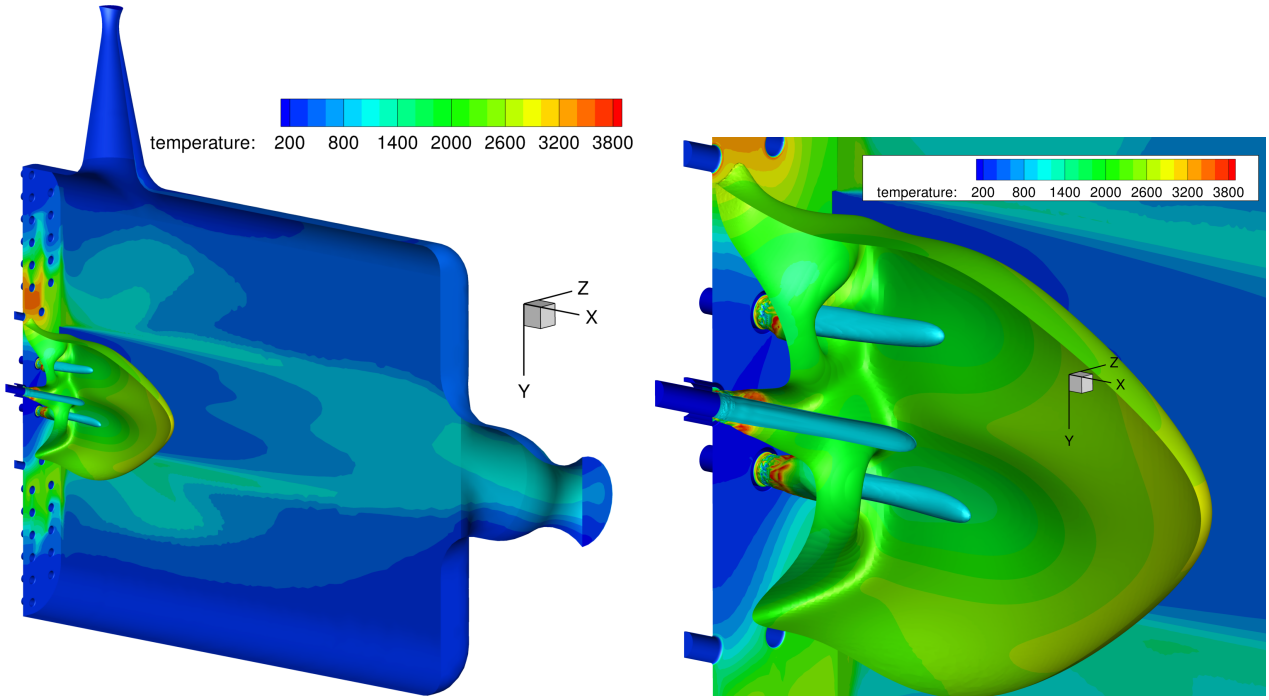

Figure 11: Steady RANS simulation results for BKH. The iso contours show flame position (stoichiometric mixture fraction value $\widetilde{Z}_{st.}$) and the Lox core density of $\rho = 250$ kg/m^3. The chamber and iso surfaces are colored by the temperature.

flame length and flame shape. In addition to that, the calculated combustion chamber pressure of 58.6 bar agrees well with the experimental value of 60.19 bar.

6. Conclusion

This paper presents a method to augment one-equation turbulence models by a separate time scale equation for flamelet combustion applications. The ω-equation from an early version of the Wilcox $k-\omega$ model is used as a passive equation of the turbulent time. The model is presented for steady Reynolds-averaged Navier-Stokes simulations but can easily be extended to DES models. Simulation results for a generic 2D test case are presented, showing that the model works in the way it was devised. In a second test case, the new model is compared to the Menter-SST turbulence model for a seven injector ideal gas test case with CH_4/O_2 combustion. This test case has been investigated numerically by several other groups and a comparison to experimental results has been published in the literature. The results for the timescale-augmented Spalart-Allmaras model agree very well with the experiments. For this test case, the new model gives slightly better results for the chamber pressure profile and the wall heat flux distribution compared to the Menter-SST model. In a last test case, the new model is applied for the simulation of a subscale combustion chamber including real gas effects and a H_2/O_2 chemistry scheme. The new timescale-augmented SA model predicts the combustion chamber pressure well and shows qualitatively good agreement for the flame length and flame shape.

7. Acknowledgements

The present work was conducted in the framework of the German Aerospace Center (DLR) project TAUROS (TAU for Rocket Thrust Chamber Simulation) focusing on the qualification and advancement of the DLR flow solver TAU for liquid rocket thrust chamber applications. The financial support of the DLR Space Research Programmatic is highly appreciated. The authors would also like to thank Justin Hardi from DLR Lampoldshausen for providing the experimental results for BKH.

DOI: 10.13009/EUCASS2019-512

References

[1] Steven R Allmaras and Forrester T Johnson. Modifications and clarifications for the implementation of the spalart-allmaras turbulence model. In *Seventh international conference on computational fluid dynamics (ICCFD7)*, pages 1–11, 2012.

[2] Satish Balay, Shrirang Abhyankar, Mark F. Adams, Jed Brown, Peter Brune, Kris Buschelman, Lisandro Dalcin, Victor Eijkhout, William D. Gropp, Dinesh Kaushik, Matthew G. Knepley, Lois Curfman McInnes, Karl Rupp, Barry F. Smith, Stefano Zampini, Hong Zhang, and Hong Zhang. PETSc users manual. Technical Report ANL-95/11 - Revision 3.8, Argonne National Laboratory, 2017.

[3] Satish Balay, William D. Gropp, Lois Curfman McInnes, and Barry F. Smith. Efficient management of parallelism in object oriented numerical software libraries. In E. Arge, A. M. Bruaset, and H. P. Langtangen, editors, *Modern Software Tools in Scientific Computing*, pages 163–202. Birkhäuser Press, 1997.

[4] Daniel T Banuti, Volker Hannemann, Klaus Hannemann, and Bernhard Weigand. An efficient multi-fluid-mixing model for real gas reacting flows in liquid propellant rocket engines. *Combustion and Flame*, 168:98–112, 2016.

[5] Scott Kenneth Beinke. *Analyses of Flame Response to Acoustic Forcing in a Rocket Combustor*. PhD thesis, School of Mechanical Engineering. The University of Adelaide. Australia., April 2017.

[6] Michael P Burke, Marcos Chaos, Yiguang Ju, Frederick L Dryer, and Stephen J Klippenstein. Comprehensive h2/o2 kinetic model for high-pressure combustion. *International Journal of Chemical Kinetics*, 44(7):444–474, 2012.

[7] Jack R Edwards and Meng-Sing Liou. Low-diffusion flux-splitting methods for flows at all speeds. *AIAA journal*, 36(9):1610–1617, 1998.

[8] Stefan Fechter, Sebastian Karl, Volker Hannemann, and Klaus Hannemann. Simulation of LOx/GH2 single coaxial injector at high pressure conditions. In *53rd AIAA/SAE/ASEE Joint Propulsion Conference*, page 4765, 2017.

[9] T. Gerhold. Overview of the hybrid RANS code TAU. In *MEGAFLOW - Numerical Simulation for Aircraft Design*, pages 81–92. Springer, 2005.

[10] RG Gilbert, K_ Luther, and J Troe. Theory of thermal unimolecular reactions in the fall-off range. ii. weak collision rate constants. *Berichte der Bunsengesellschaft für physikalische Chemie*, 87(2):169–177, 1983.

[11] Justin Hardi. *Experimental Investigation of High Frequency Combustion Instability in Cryogenic Oxygen-Hydrogen Rocket Engines.* PhD thesis, School of Mechanical Engineering. University of Adelaide. South Australia 5005. Australia, 2012.

[12] Tim Horchler, Kai Oßwald, Volker Hannemann, and Klaus Hannemann. Hybrid rans-les study of transonic flow in the wake of a generic space launch vehicle. In *Symposium on Hybrid RANS-LES Methods*, pages 291–300. Springer, 2016.

[13] Matthias Ihme and Yee Chee See. Prediction of autoignition in a lifted methane/air flame using an unsteady flamelet/progress variable model. *Combustion and Flame*, 157(10):1850–1862, 2010.

[14] Seong-Ku Kim, Hwan-Seok Choi, and Yongmo Kim. Thermodynamic modeling based on a generalized cubic equation of state for kerosene/lox rocket combustion. *Combustion and flame*, 159(3):1351–1365, 2012.

[15] Guilhem Lacaze and Joseph C Oefelein. A non-premixed combustion model based on flame structure analysis at supercritical pressures. *Combustion and Flame*, 159(6):2087–2103, 2012.

[16] Meng-Sing Liou. A sequel to AUSM, Part II: AUSM+-up for all speeds. *Journal of computational physics*, 214(1):137–170, 2006.

[17] Johannes Löwe, Axel Probst, Tobias Knopp, and Roland Kessler. A low-dissipation low-dispersion second-order scheme for unstructured finite-volume flow solvers. In *53rd AIAA Aerospace Sciences Meeting*, page 0815, 2015.

[18] Johannes Löwe, Axel Probst, Tobias Knopp, and Roland Kessler. Low-dissipation low-dispersion second-order scheme for unstructured finite volume flow solvers. *AIAA Journal*, pages 2961–2971, 2016.

[19] Peter C. Ma, Daniel T. Banuti, Jean-Pierre Hickey, and Matthias Ihme. Numerical framework for transcritical real-fluid reacting flow simulations using the flamelet progress variable approach. In *55th AIAA Aerospace Sciences Meeting*, number 2017-0143, 2017.

[20] A. Mack and V. Hannemann. Validation of the unstructured DLR-TAU-Code for hypersonic flows. In *32nd AIAA Fluid Dynamics Conference and Exhibit*, St. Louis, Missouri, 2012.

[21] Florian R Menter, Martin Kuntz, and Robin Langtry. Ten years of industrial experience with the sst turbulence model. *Turbulence, heat and mass transfer*, 4(1):625–632, 2003.

[22] Kai Oßwald, Alexander Siegmund, Philipp Birken, Volker Hannemann, and Andreas Meister. L2Roe: a low dissipation version of Roe's approximate Riemann solver for low mach numbers. *International Journal for Numerical Methods in Fluids*, 81(2):71–86, 2016.

[23] Nikolaos Perakis, Oskar J Haidn, Daniel Eiringhaus, Daniel Rahn, Silong Zhang, Yu Daimon, Sebastian Karl, and Tim Horchler. Qualitative and quantitative comparison of rans simulation results for a 7-element gox/gch4 rocket combustor. In *2018 Joint Propulsion Conference*, page 4556, 2018.

[24] Heinz Pitsch. *Entwicklung eines Programmpakets zur Berechnung eindimensionaler Flammen am Beispiel einer Gegenstromdiffusionsflamme.* Diplomarbeit, Rheinisch-Westfälische Technische Hochschule Aachen, 1993.

[25] Cord-Christian Rossow. Extension of a compressible code toward the incompressible limit. *AIAA journal*, 41(12):2379–2386, 2003.

[26] Ralf Rudnik. Untersuchung der Leistungsfähigkeit von Zweigleichungs-Turbulenzmodellen bei Profilumströmungen. DLR-Forschungsbericht DLR-FB-97-49, Deutsches Zentrum für Luft- und Raumfahrt, 1997.

[27] Anthony M Ruiz, Guilhem Lacaze, Joseph C Oefelein, Raphaeë Mari, Bénédicte Cuenot, Laurent Selle, and Thierry Poinsot. Numerical benchmark for high-reynolds-number supercritical flows with large density gradients. *AIAA Journal*, 54(5):1445–1460, 2015.

[28] D. Schwamborn, T. Gerhold, and R. Heinrich. The DLR-TAU-Code: Recent applications in reasearch and industry. In *Proceedings of the European Conference on Computational Fluid Dynamics (ECCOMAS).*, 2006.

[29] Simona Silvestri, Maria Palma Celano, Gregor Schlieben, and Oskar J Haidn. Characterization of a multi-injector gox/ch4 combustion chamber. In *52nd AIAA/SAE/ASEE Joint Propulsion Conference*, page 4992, 2016.

[30] Gregory P Smith, David M Golden, Michael Frenklach, Nigel W Moriarty, Boris Eiteneer, Mikhail Goldenberg, C Thomas Bowman, Ronald K Hanson, Soonho Song, WC Gardiner Jr, et al. Gri-mech 3.0, 1999. *URL http://www. me. berkeley. edu/gri_mech*, 2011.

[31] Charles G Speziale, Ridha Abid, and E Clay Anderson. Critical evaluation of two-equation models for near-wall turbulence. *AIAA journal*, 30(2):324–331, 1992.

[32] TAU Entwicklergruppe. Tau user guide, release 2017.1.0. Technical report, Institut für Aerodynamik und Strömungstechnik. Deutsches Zentrum für Luft- und Raumfahrt, 2017.

[33] B. Thornber, A. Mosedale, D. Drikakis, D. Youngs, and R.J.R. Williams. An improved reconstruction method for compressible flows with low mach number features. *Journal of Computational Physics*, 227(10):4873 – 4894, 2008.

[34] Tamás Turányi and Alison S Tomlin. *Analysis of kinetic reaction mechanisms*. Springer, 2014.

[35] David C Wilcox. Reassessment of the scale-determining equation for advanced turbulence models. *AIAA journal*, 26(11):1299–1310, 1988.

[36] David C. Wilcox. *Turbulence Modeling for CFD*. DCW Industries, 3rd edition, 2006.

[37] CR Wilke. A viscosity equation for gas mixtures. *The journal of chemical physics*, 18(4):517–519, 1950.

[38] L. Zipperer and F. Herning. Beitrag zur Berechnung der Zähigkeit technischer Gasgemische aus den Zähigkeitswerten der Einzelbestandteile. *Das Gas- und Wasserfach*, 1936.